Quantifying the variability in water use efficiency from the canopy to ecosystem scale across main croplands

Quantifying the variability in water use efficiency from the canopy to ecosystem scale across main croplands

Yanan Chen [a, b], Zhi Ding [a, b], Pujia Yu [a, b], Hong Yang [c], Lisheng Song [a, b], Lei Fan [a, b], Xujun Han [a, b], Mingguo Ma [a, b], Xuguang Tang [a, b,*]

[a] Chongqing Jinfo Mountain Karst Ecosystem National Observation and Research Station, School of Geographical Sciences, Southwest University, Chongqing 400715,

China

[b] Chongqing Engineering Research Center for Remote Sensing Big Data Application, School of Geographical Sciences, Southwest University, Chongqing 400715, China

[c] Department of Geography and Environmental Science, University of Reading, Whiteknights, Reading RG6 6AB, UK

* Corresponding author at: Chongqing Jinfo Mountain Karst Ecosystem National Observation and Research Station, School of Geographical Sciences, Southwest University, Chongqing 400715, China.

E-mail address: xgtang@swu.edu.cn (X. Tang).

Abstract

Current, how to use limited water resources efficiently and improve agricultural water use efficiency, has become one of the greatest challenges for global food security. In this study, multiple site-years of carbon and water flux data across the major crops including maize, winter wheat and soybean, were used to quantify the variability in canopy-scale transpiration (T), ecosystem-scale evapotranspiration (ET) as well as the associated water use efficiencies (WUE_T and WUE_{ET}). On the basis of ET partitioning, the results indicated that the transpiration ratio–T/ET as well as T and ET exhibited an obvious single-peak seasonal pattern across the typical croplands. However, at the early and late growing stages, there existed large discrepancies in T and ET owing to low vegetation coverage, while T and ET were very close during the peak period. Among them, maize exhibited the largest T/ET by 0.50 ± 0.12, followed by soybean of 0.43 ± 0.08 and winter wheat of 0.38 ± 0.09, respectively. Furthermore, the coupling relationships between gross primary productivity (GPP) and water fluxes including T and ET changed from linear to nonlinear. The study also found that the variability in WUE_T and WUE_{ET} were not consistent. Specifically, WUE_{ET} showed distinct seasonal characteristic whereas WUE_T kept constant as a plateau almost throughout the growth period, which reflected the inherent physiological property controlled by plant stomata at the canopy scale. Among these crops, maize exhibited the largest WUE_T and WUE_{ET} (5.30 ± 0.89 and 2.48 ± 1.14 g C kg^{-1} H_2O), followed by winter wheat (4.97 ± 1.52 and 2.35 ± 0.64 g C kg^{-1} H_2O) and soybean (4.88 ± 1.59 and 1.89 ± 0.99 g C kg^{-1} H_2O), respectively.

1. Introduction

Detection of impacts on agriculture caused by global climate change has increased substantially in the past decades, which is critical for designing and evaluating climate mitigation and adaptation measures (Song et al., 2021). With increasing global surface temperature, terrestrial ET generally increased and soil moisture reduced, resulting in the available water resource more stressed in agricultural ecosystems and decreasing grain reserves seriously (Jiang, 2009; Liu et al., 2016; Ullah et al., 2019). Therefore, the widespread, rapid and intensifying climate change has threatened global food security. As a result of global population increase and changing demand, how to use limited water re- sources more efficiently and improve agricultural water use efficiency has become the focus of grain production (Wallace, 2000; Dietzel et al., 2016; Wang et al., 2018).

Water use efficiency (WUE) reflects the capacity of croplands to produce biomass through vegetation photosynthesis per unit of water consumption by plant T or ecosystem-level ET (Tang et al., 2014). Depending on different research scales, cropland WUE can be divided into three levels: leaf, canopy and ecosystem (Blum, 2005; Niu et al., 2011). As an especially important determinant of crop productivity, the variability in WUE describes the tradeoff process between water loss and carbon sequestration (Lan et al., 2021). Specifically, carbon uptake by plant photosynthesis was accompanied by water dissipation to regulate the water-carbon balance between the terrestrial biosphere and atmosphere (Berry et al., 2010; Mu et al., 2011; Ito and Inatomi, 2012). All these carbon and water cycling processes are essentially vulnerable to the effect of environmental changes, especially for the semi-artificial cropland ecosystems (Scanlon and Albertson, 2004; Xu et al., 2018). In the field, some farmers have to reduce water use and select drought-resistant crops, achieving water-saving agriculture (Zhao et al., 2017).

The eddy covariance-based flux towers can directly and continuously measure terrestrial carbon and water fluxes at site scale, which provides a feasible way to monitor the key processes of ET and WUEET (WUEET =GPP/ET) of farmland ecosystems (Yu et al., 2014; Tang et al., 2015). Currently, a few flux sites have been established at the main croplands including corn, soybean, and wheat. Such observations can be further processed to standardized GPP and ET products (Zhou et al., 2015; Tang et al., 2017). Essentially, water loss through ET in agroecosystem was mainly comprised of plant T and soil evaporation (E) (Fisher et al., 2008; Maxwell and Condon, 2016). Moreover, T is recognized as the dominant component of ET, which is more related to vegetation growth and biomass accumulation (Schlesinger and Jasechko, 2014; Cheng et al., 2017; Ren et al., 2019). Therefore, it is especially important to improve the inherent WUET (WUET =GPP/T) at the canopy scale to alleviate the current water crisis for food security.

Nevertheless, direct measurement of the canopy T from cropland remained difficult and complicated (Scott et al., 2017). Effectively separating the components of ET is a challenge in the field of hydro- meteorology, which even constrained the deep understanding of interactions between carbon and water cycles (Scanlon, 2008; Scanlon and Kustas, 2010). Currently, several methods including micro lysimeter, sap flow, stable isotope and eddy covariance techniques have been developed to measure soil evaporation (E), vegetation transpiration (T) and ET (Wang et al., 2010; Xiao et al., 2018; Paul-Limoges et al., 2020). However, the micro-lysimeter method neglected canopy interception evaporation, leading to larger estimation of transpiration (Liu et al., 2002). Large uncertainty existed in the isotope method for ET partitioning owing to a series of assumptions. Especially when soil evaporation was small, this technique was not suitable for agricultural and forest ecosystems (Griffis, 2013; Good et al., 2014). Sap flow can continuously record stand-level transpiration, but it is difficult to scale up to large scales (Rafi et al., 2019). Nowadays the eddy covariance-based flux data has been used for partitioning ET with relatively accurate results, but this method was not widely adopted since it required high frequency (10–20 Hz) data that is only available to tower owners (Baldocchi and Ryu, 2011; Wagle et al., 2020). A simple method using the

widely available half-hourly flux data would contribute to ET partitioning for different ecosystems. Based on the concept of underlying water use efficiency (uWUE), Zhou et al. (2018) developed a novel partitioning method which can estimate T/ET at various spatiotemporal scales and is simple to apply in practice (Jiang et al., 2020; Nelson et al., 2020).

Since the beginning of the COVID-19 pandemic globally, jointly with the effects of natural disasters such as locust plague, drought and flood worldwide, the agricultural production is disturbed seriously which even endangers human survival (Monfreda et al., 2008). As the world's major food crops, maize is one of the most widely produced and consumed cereal crops, followed by wheat, and soybean is a high protein plant that people can prepare and eat in a variety of ways. To deeply reveal the underlying processes and mechanisms of water and carbon cycles during grain production for improving agricultural water use efficiency, we partitioned ecosystem-level ET based on the concept of underlying water use efficiency and continuous flux observations across the major crop sites. The overall aims of this study were: 1) to characterize the seasonal dynamics of T/ET for the maize, wheat and soybean croplands as well as their differences during the growing period; 2) to analyze the variability in site-level GPP and water loss from the canopy (T) to ecosystem scale (ET) as well as the carbon-water coupling relationship; 3) to have a better understanding of the carbon-water interactions by means of WUE_T and WUE_{ET} over crop species; and 4) to reveal the underlying influencing factors controlling the transpiration ratio (T/ET), WUE_T and WUE_{ET} among the three typical cropland eco- systems. All these analyses are of great significance for understanding the processes of cropland evapotranspiration, and sustainable use of water resources for global food security.

2. Methods and materials

2.1 Description of the flux sites

A total of 9 flux sites across three typical croplands (soybean, maize, winter wheat) were used for analysis in the study (Table 1), which can be accessed from the AmeriFlux, ChinaFlux and European flux network. The geographical locations of all sites were also showed in Fig. S1. The soybean flux sites are comprised of US-Br3, US-Ne3 and US-Bo1. The US- Br3 site is located in central Iowa, USA, with hot and humid climate in summer and soybean was planted in the odd years (John and Tim, 2016). The US-Bo1 site lies in the Midwestern part of the USA, Illinois. The field cultivated soybean in the even years with temperate continental climate (Tilden, 2016). The US-Ne3 flux site is placed in the University of Nebraska Agricultural Research and Development Center near Mead, Nebraska, USA. This area has similar cropping management as US-Bo1 where soybean was planted in the even years. Besides, both US-Ne3 and US-Bo1 sites rely on natural rainfall for irrigation (Suyker, 2021).

Table 1

Description of the tower-based flux sites of croplands used in this study.

Crop type	Site ID	Latitude (°)	Longitude (°)	MAP (mm)	MAT (°C)	Available years	References
Soybean	US-Br3	41.9747	-93.6936	846.6	8.90	2005/2007/2009	(Chu et al., 2018)
	US-Ne3	41.1797	-96.4397	783.7	10.11	2008/2010/2012	(Novick et al., 2016)
	US-Bo1	40.0062	-88.2904	991.0	11.00	2002/2004/2006	(Meyers and Hollinger, 2004)
Maize	US-Ne1	41.1651	-96.4766	790.4	10.07	2009–2011	(Barr et al., 2013)
	CN-Yuc	36.8290	116.5702	582.0	13.10	2007–2009	(Yu et al., 2006)
	CN-Daman	38.8556	100.3722	126.7	7.20	2013–2015	Song et al. (2016)
Winter wheat	CN-Yuc	36.8290	116.5702	582.0	13.10	2007–2009	(Ailin et al., 2016)
	DE-Seh	50.8706	6.4497	693.0	9.90	2007/2008, 2008/2009	(Schmidt et al., 2012)
	US-ARM	36.6058	-97.4888	843.0	14.76	2006/2007, 2009/2010	(Lu et al., 2017)

Note: MAP and MAT represent multi-year mean precipitation and temperature, respectively.

Three flux sites of maize were used for analysis including CN-Daman, US-Ne1 and CN-Yuc. The CN-Daman site lies in the farmland of Daman Irrigation District in Zhangye City, Gansu Province, China, where has been observed since June 2012. The climate of the region can be characterized as temperate continental arid with abundant heat and light, dry and little rain (Liu et al., 2013). The US-Ne1 is an irrigated continuous maize site, one of three experimental fields (US-Ne1, US-Ne2 and US-Ne3) located within 1.6 km of each other (Suyker, 2021). The last corn site is CN-Yuc, which is situated in the southwest of Yucheng City, Shandong Province, China. The area belongs to warm temperate semi-humid monsoon climate, with abundant supply of light, heat and rainfall occurring in the same period. Generally, winter wheat and summer corn are planted in Yucheng station.

Three winter wheat sites were comprised of CN-Yuc, DE-Seh and US- ARM. Detailed information about the CN-Yuc site has been described above. The Selhausen test site (De-Seh) belongs to the southern part of the Lower Rhine Embayment and near the Belgium boundary with temperate maritime climate (Schmidt et al., 2012; Wang et al., 2018). This area is a rotation field, and winter wheat was planted from October 2007 to October 2009. The US-ARM site with humid subtropical climate is situated in northern Oklahoma, USA. In the field, winter wheat, corn, soy and alfalfa have been planted in different years, and we only used the winter wheat years for analysis (Lu et al., 2017; Wang et al., 2018).

2.2 Flux data preprocessing

For each flux site, the eddy-covariance system continuously records net ecosystem carbon exchange (NEE) and latent heat (LE) at a frequency of 10 Hz. Meanwhile, the meteorological data including solar radiation, air temperature (Ta), soil temperature/moisture, wind speed/ direction, relative humidity (RH) and precipitation are measured at these cropland sites. In addition to careful instrument maintenance and periodic calibration, the standardized procedures require spike detection, lag correction for H_2O/CO_2 relative to the vertical wind component, density fluctuation correction (WPL correction), sonic virtual temperature correction, and frequency response correction (Song et al., 2016; Liu and Xu, 2018). These 10 Hz data were then processed into half-hour products by the Edire post-processing software (University of Edinburgh, Edinburgh, UK). Gap-filling and flux partitioning by the nighttime-based method were carried out with the R package by the Max Planck Institute for Biogeochemistry (https://www.bgc-jena.mpg. de/bgi /index.php/Services/ REddyProcWeb) (Reichstein et al., 2014; Wang et al., 2018).

The half-hourly GPP, ET and VPD data were used for ET partitioning. Therefore, the flux partition method proposed by Reichstein et al. (2005) was used to separate NEE into the GPP and ecosystem respiration (R_e). GPP was calculated as the sum of observed daytime NEE and modeled R_e inferred from night-time NEE. The partitioning algorithm extrapolates night-time values of R_e into the daytime based on short-term temperature sensitivity of R_e. The flow chart of data preprocessing can be seen in Fig. S2. Then, the measured latent heat (LE, W/m^2) fluxes were derived to obtain water consumption (ET, mm/day) by multiplying a factor of 0.035 which was converted by the formula ET=LE/λ (λ represents amount of energy to evaporate per unit weight of water; 2,454,000 J kg^{-1}) (Tang et al., 2014, Wang et al., 2018). At canopy or ecosystem scales, vapor pressure deficit (VPD) is almost the same within a uniform environment, and it can be calculated by Ta and RH data from the flux site (Romero-Aranda et al., 2006). In addition, in order to partition ET into E and T, data screening and quality control were performed to select half-hourly observations in accordance to the following criteria: 1) the daylight GPP, ET, and VPD data were used while defective entries were excluded; 2) data from rainy days were excluded; 3) sensible heat flux larger than 5 W m^{-2} and incoming shortwave radiation larger than 50 W m^{-2} were used to avoid stable boundary layer conditions; 4) data were selected for each site during the growing season; 5) 8-day T/ET values were estimated at least 80 effective entries (Zhou et al., 2016, Li et al., 2019).

2.3 MODIS data preparation

The normalized vegetation index (NDVI) has been widely used to describe the vegetation growth at different spatial and temporal scales (Pettorelli et al., 2005; Wardlow and Egber, 2008). In this study, we used the MOD09A1 product (V6) over an 8-day interval to calculate time-series NDVI (https://e4ftl01.cr.usgs.gov/MOLT/MOD09A1.006/), and then derive crop phenological information. MOD09A1 provides an estimate of the surface spectral reflectance of bands 1–7 at 500 m resolution corrected for atmospheric conditions such as gases, aerosols, and Rayleigh scattering. The near-infrared band and red band were used to calculate NDVI (Gillies et al., 1997; Zhang et al., 2006).

The TIMESAT program developed by Department of Earth and Eco- systems Sciences, Lund University was used to extract the phenological parameters including start of growing season (SOS), end of growing season (EOS) and length of the crop growing season. Due to noise of the clouds and atmosphere, it is important to fit and reconstruct the time- series NDVI data (Gu et al., 2009). In this study, we used the asymmetric Gaussian function and a sliding window to obtain the valley and peak values of the NDVI curves (Cai et al., 2017). Furthermore, SOS and EOS were defined as 20% of which multiplied by the amplitude of the

left and right halves, respectively using the dynamic threshold method. Fig. 1 showed the process of extraction at the CN-Daman site in 2013, and the other sites were analyzed using the same method. Noteworthy, SOS of winter wheat was defined at the date when the wheat turned green after winter dormancy (Zhou et al., 2013; Guo et al., 2016).

Leaf area index (LAI) quantifies the amount of leaf area in an ecosystem and is a critical variable in processes such as photosynthesis, evapotranspiration, and precipitation interception (Alton, 2016). The study used the MOD15A2H LAI (V6) dataset at 8-day intervals to analyze the effect of vegetation status on the variability in T/ET at all cropland sites. MOD15A2H algorithm exploited the spectral information including MODIS red and near-infrared surface retrieved reflectance, and a radiative transfer equation generated based a look-up table (Knyazikhin et al., 1998), which has experienced substantial improve- ments till now (Fang et al., 2019).

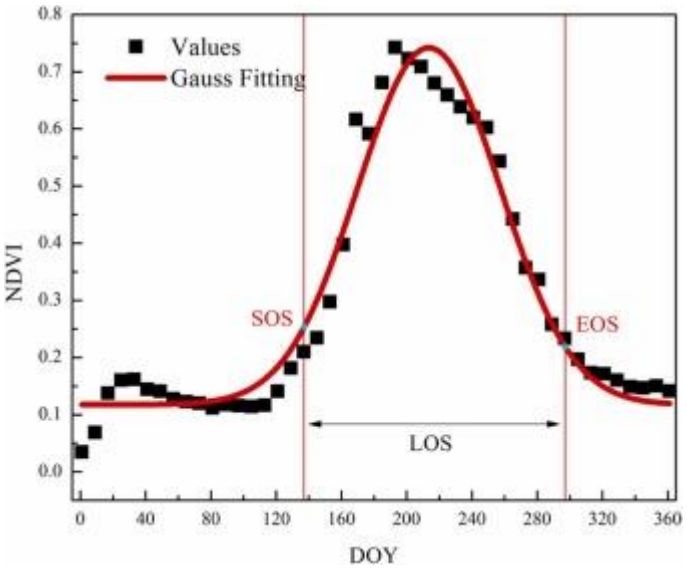

Fig. 1. Deriving the crop phenological information from time-series MODIS NDVI data. Two blue marked points represent SOS and EOS, respectively. The black line was LOS (length of growing season) and DOY meant day of year.

2.4 Process for partitioning ET

Water consumptions from E, T, and ET are essentially associated with non-stomatal, stomatal, and stomatal/non-stomatal mixing behaviors, respectively (Zhu et al., 2015; Drake et al., 2017). T is controlled by stomatal regulation, whereas E is only related to soil and environmental conditions. The concept of WUE includes ecosystem-level WUE (WUE_{ET}) and canopy-scale transpiration efficiency (WUE_T). WUE_{ET} is defined as carbon uptake (GPP) per unit of water loss by ET, and WUE_T is defined as GPP per unit of water loss through T. Thus, the ratio of WUE_{ET} to WUE_T can be determined by T/ET. WUE_{ET} can be calculated directly from tower-based flux observations, which made T/ET crucial to derive WUE_T. Referring to the novel partitioning method developed by Zhou et al. (2018), this study also defined the uWUEp and uWUEa to represent the potential water use efficiency and apparent water use efficiency, respectively. Here, T/ET can be calculated by dividing uWUEa to uWUEp as follows.

The uWUEp and uWUEa were estimated with all and 8-day period half-hourly GPP, VPD and ET data at the cropland sites using the quantile regression and linear regression method, respectively. In addition, the intercepts of both quantile and linear regressions were set to zero. Taking the site US-Ne3 as an example (Fig. 2a), the long-term mean uWUEp

was estimated as the regression slope of the 95th quan- tile regression using all half-hourly data from the site. Therefore, the uWUEp was 12.28 g C $hPa^{0.5}$/kg H_2O. Then, the regression slope using half-hourly data for a particular 8 day period was estimated to represent a typical 8 day uWUEa value for the site. As shown in Fig. 2b, the value was 6.67 g C $hPa^{0.5}$/kg H_2O for DOY 193–200 in 2008. So, the ratio of T/ET was 0.54 for the 8 day period.

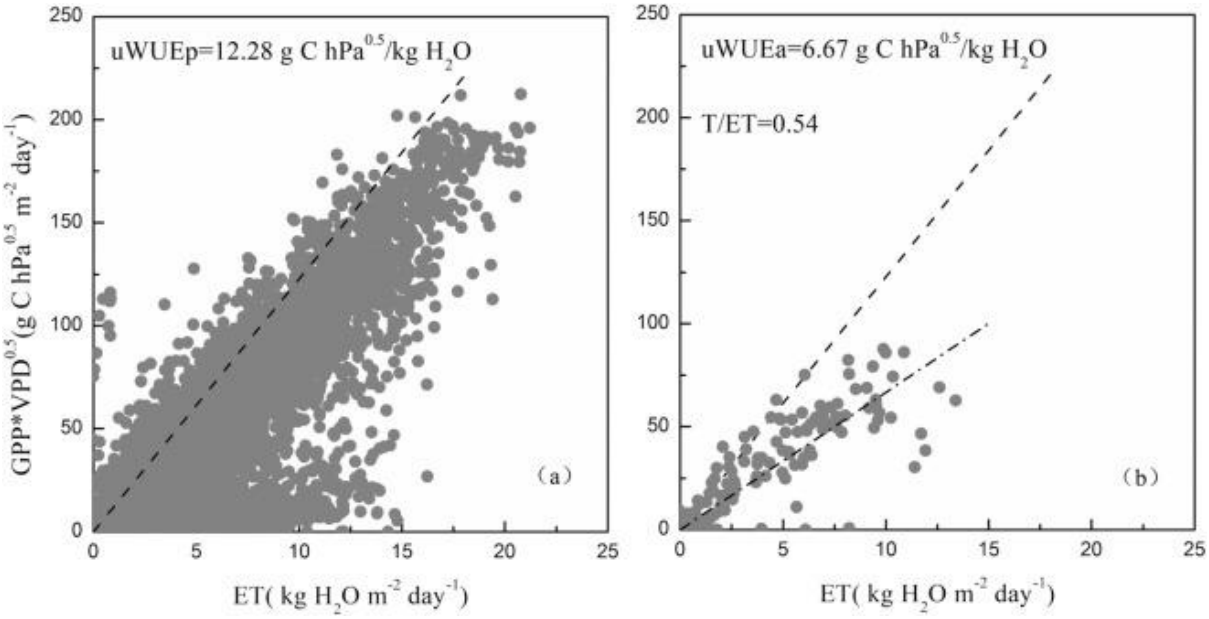

Fig. 2. The 95th quantile regression using all the half-hourly data for the US-Ne3 site (a) and the linear regression using half-hourly data from DOY 193–200 in 2008 (b). The intercept was set to zero for both quantile and linear regressions.

2.5 Statistical analysis

Two models including quantile regression and linear regression were used to derive the values of uWUEp and uWUEa by SPSS 26.0 (Chicago, IL, USA), respectively. Then we can acquire the seasonal variations in T/ ET for each flux site. To test the relationship between T/ET and LAI across these typical croplands, the regression model jointly with rele- vant coefficient of determination (R^2) were used for evaluation. R^2 indicated the overall explanatory ability of regression model in explaining the variability of T/ET data. Subsequently, to reveal the differences in response mechanism of WUE_T and WUE_{ET} to GPP, T and ET among different crops, the Pearson correlation coefficient (r) was performed. Generally, a value of r close to 1 indicated a strong positive linear relationship as it passed the significance test.

3. Results

3.1 T/ET of typical croplands over 8 day period

Fig. 3 illustrated the seasonal variations in T/ET across the typical cropland sites including soybean, maize and winter wheat, respectively. As a proxy for the transpiration ratio, T/ET exhibited a single-peak curve over all these crops, which was also well captured by the time-series MODIS LAI data. At the soybean and maize sites, T/ET nearly co- varied with LAI over

an 8-day interval. As the crops grew, both T/ET and LAI increased rapidly from the end of April, reached the peaks in July of the year, and then gradually decreased with leaf withering in autumn (Fig. S3). Owing to different agricultural planting systems, the main growing period of winter wheat is the first half of next year after winter dormancy. Similar to the other crops, the variability in T/ET also exhibited an obvious single-peak pattern and climbed to the maximum around mid-April. Therefore, this study confirmed that T/ET varied consistently with LAI across all cropland sites.

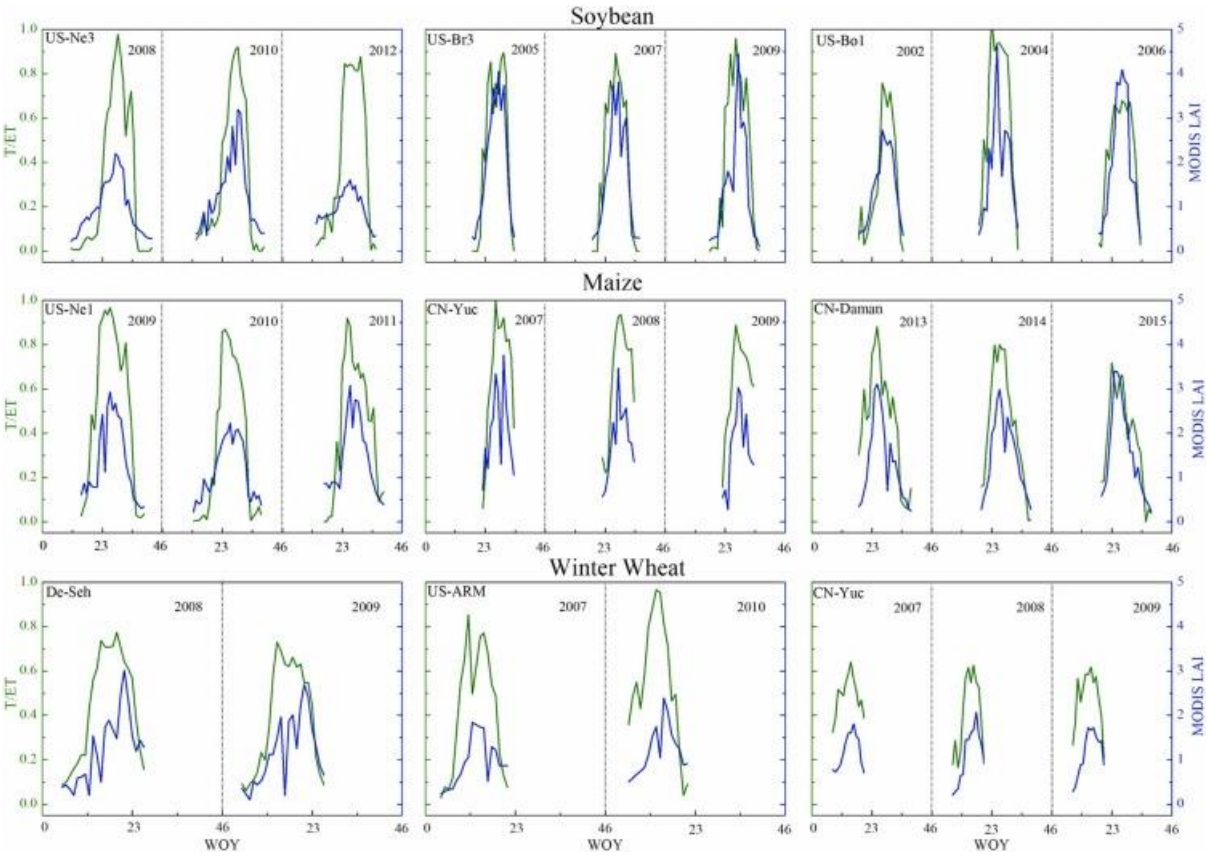

Fig. 3. Seasonal variations in T/ET at the typical cropland flux sites during the growing season. WOY meant week of year at 8-day period.

Nevertheless, the magnitudes of T/ET have contrasting heterogeneity because of differences in crop species, climate zones and irrigation regimes. Especially for the CN-Yuc site, winter wheat–maize double cropping is an important rotation system in the North China Plain, which resulted in larger T/ET for both maize and winter wheat compared to other sites (Fig. 4). Despite of the same environment conditions between the US-Ne3 and US-Ne1 sites, multi-year mean T/ET of soybean was obviously lower than that of maize by 21.9%, which proved that C_4 crop has relatively higher T/ET value in comparison with C_3 crop. The low T/ET at the CN-Daman maize site can be ascribed to the effect of arid climate characteristic in this region. Overall, multiple site-years of flux data inferred that maize has the largest T/ET by 0.50, followed by soybean of 0.43 and winter wheat of 0.38, respectively.

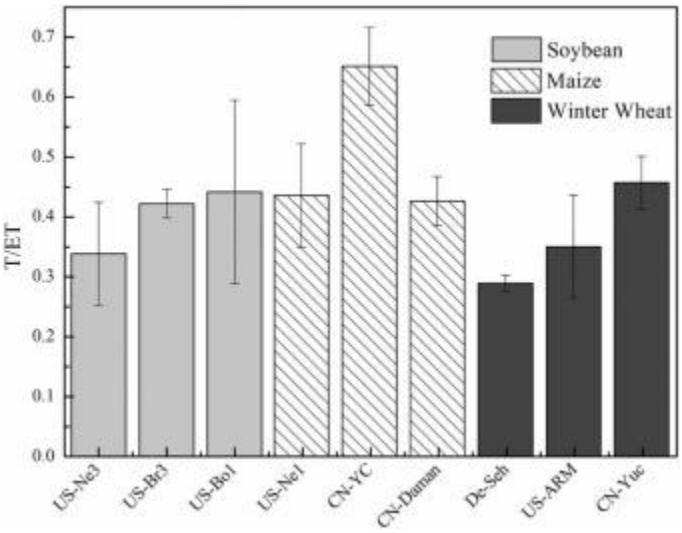

Fig. 4. Differences in multi-year mean T/ET across the typical cropland sites including soybean, maize, and winter wheat. Error bars represented ± 1 standard error.

3.2 Seasonal variations in GPP, ET and T of typical croplands

Dynamics of GPP, ET and T over an 8-day period for soybean, maize and winter wheat croplands exhibited distinct seasonal trends (Fig. 5). On the onset time when seeds of soybean and maize are sown in spring, the photosynthetic activity of vegetation was weak. Subsequently, GPP gradually increased with crop growth, reached peak in summer (approximately WOY27) and decreased again as the crop matured in autumn. However, the seasonality of winter wheat was entirely different. The GPP values were close to 0 g C m^{-2} d^{-1} during winter dormancy, increased rapidly as the temperature rose in spring, peaked in early May, and then gradually decreased till the start of June (US-ARM and CN-Yuc) or July (DE-Seh). Despite of different magnitudes, the variabilities in T and ET at the three crops also showed similar seasonal patterns to GPP. Both ET and T changed jointly with GPP. Meanwhile, this study found that the maximum GPP of maize (C_4 crop) was apparently larger than that of the other C_3 crops (26.1 g C m^{-2} d^{-1} against 17.4 g C m^{-2} d^{-1}), due to stronger carbon sequestration capacity. In addition, the results showed the largest GPP, ET and T values in maize crops for all sites with 8.96 ± 2.17 g C m^{-2} d^{-1}, 3.03 ± 0.35 and 1.70 ± 0.27 mm d^{-1}, followed by winter wheat (7.62 ± 2.60 g C m^{-2} d^{-1}, 2.67 ± 0.72 and 1.34 ± 0.32 mm d^{-1}), with the lowest values in soybean of 5.78 ± 1.95 g C m^{-2} d^{-1}, 2.4 ± 0.28 and 1.30 ± 0.27 mm d^{-1}. During the early and late stages of growing period, owing to low vegetation coverage, the water consumed by soil evaporation occupied a large proportion of ET. However, as vegetation grew, the water consumed by vegetation T gradually exceeded soil evaporation, and became the main component of ET. Then, T and ET were very close at the peak period with the relative difference of 15.6 ± 11.8%.

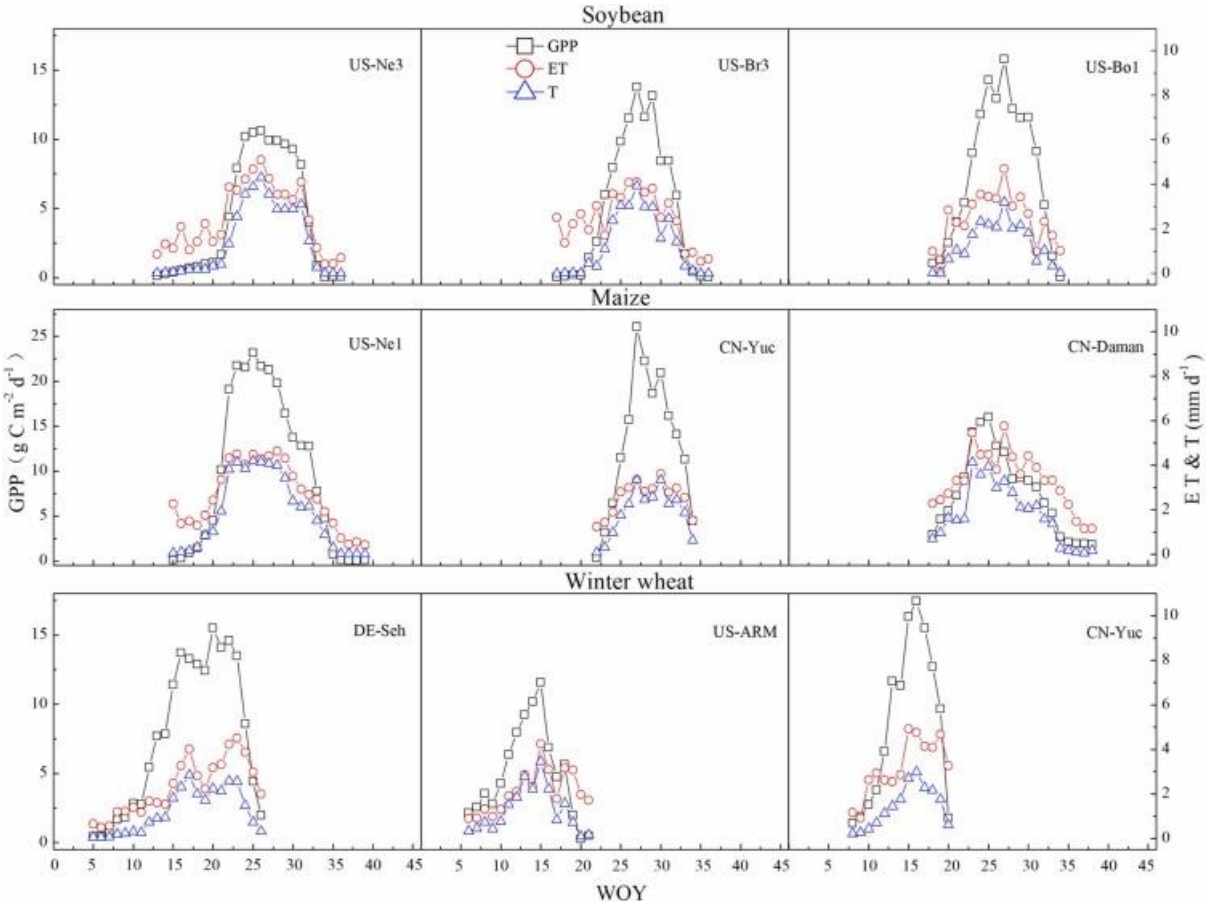

Fig. 5. Seasonal variations of tower-based GPP, ET and T at the typical cropland sites.

The study also examined the pattern of the water-carbon relationship at these cropland sites in Fig. 6. During the whole growing season for all sites, 8-day GPP and T presented a strong positive linear correlation, while 8-day GPP and ET showed significant nonlinear relationship, with R^2 of 0.81 and 0.54, respectively. Generally, the almost synchronous variation between GPP and ET and between GPP and T, as well as the primary control of canopy development and senescence, induced a close water-carbon coupling. However, GPP and T indicated a significant positive correlation than the nonlinear relationship of GPP and ET due to the high ET during early and late growing seasons (Fig. 5). Specially, the C_4 cropland–maize had a maximum R^2 with 0.84, followed by the C_3 cropland including winter wheat (0.83) and soybean (0.80).

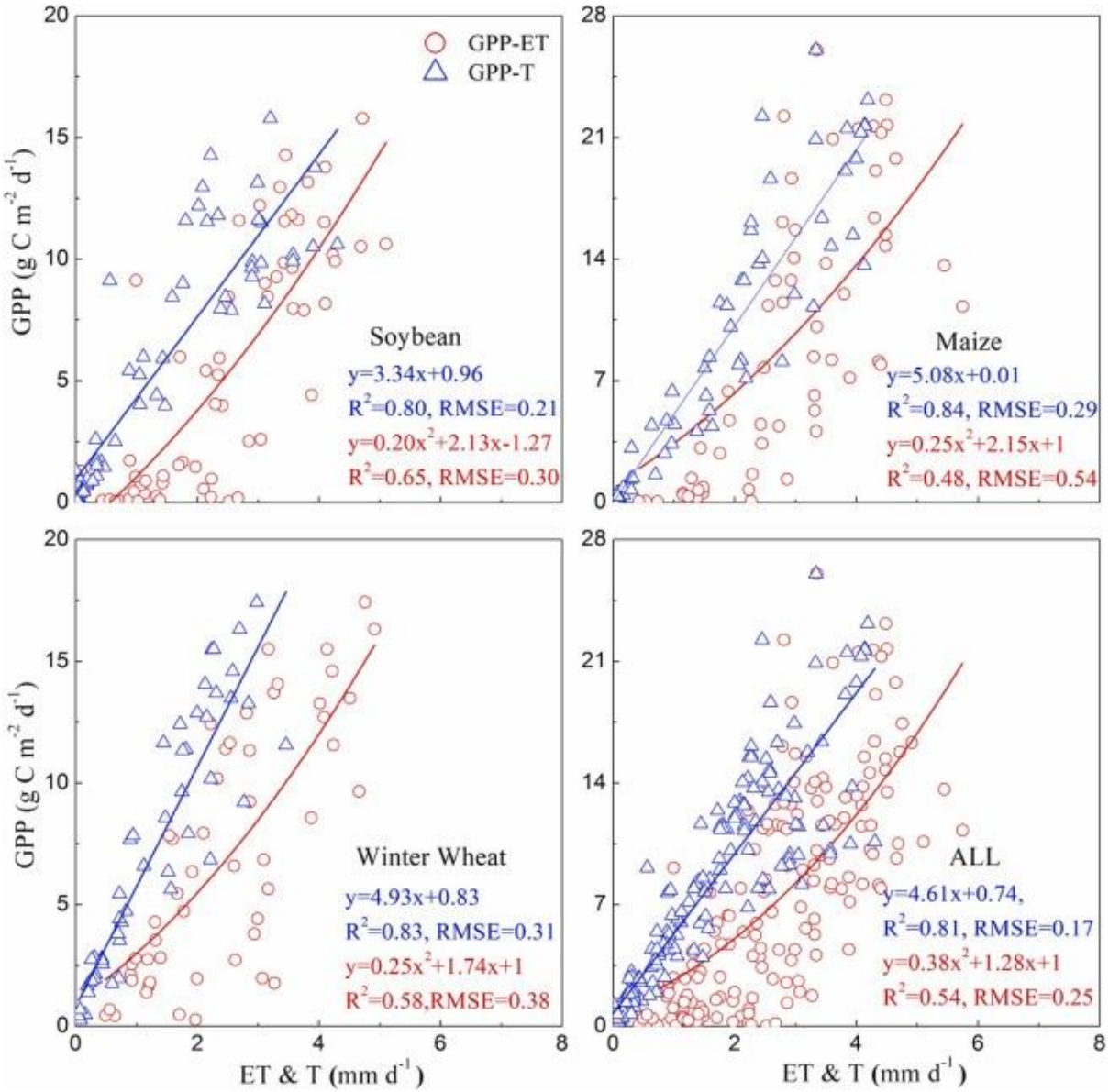

Fig. 6. Regression relationships between 8-day GPP and ET or T during the whole growing season at soybean, maize and winter wheat sites, respectively.

3.3 Comparison between WUE_T and WUE_{ET}

The variability in WUE_T and WUE_{ET} at three typical croplands were shown in Fig. 7, which illustrated the water-carbon relationships and variations from the canopy to ecosystem scale. Overall, WUE_{ET} at the soybean, maize and winter wheat sites had significant seasonal dynamics over an 8-day interval during the growing period. Contrastingly, WUE_T kept constant as a plateau in the middle stage of crop growing season, which reflected the inherently coupling relations to GPP through plant stomata at the canopy scale. The extremely low GPP or T at the beginning and ending of crop growing season can explain large fluctuations or anomalous values in WUE_T over such period.

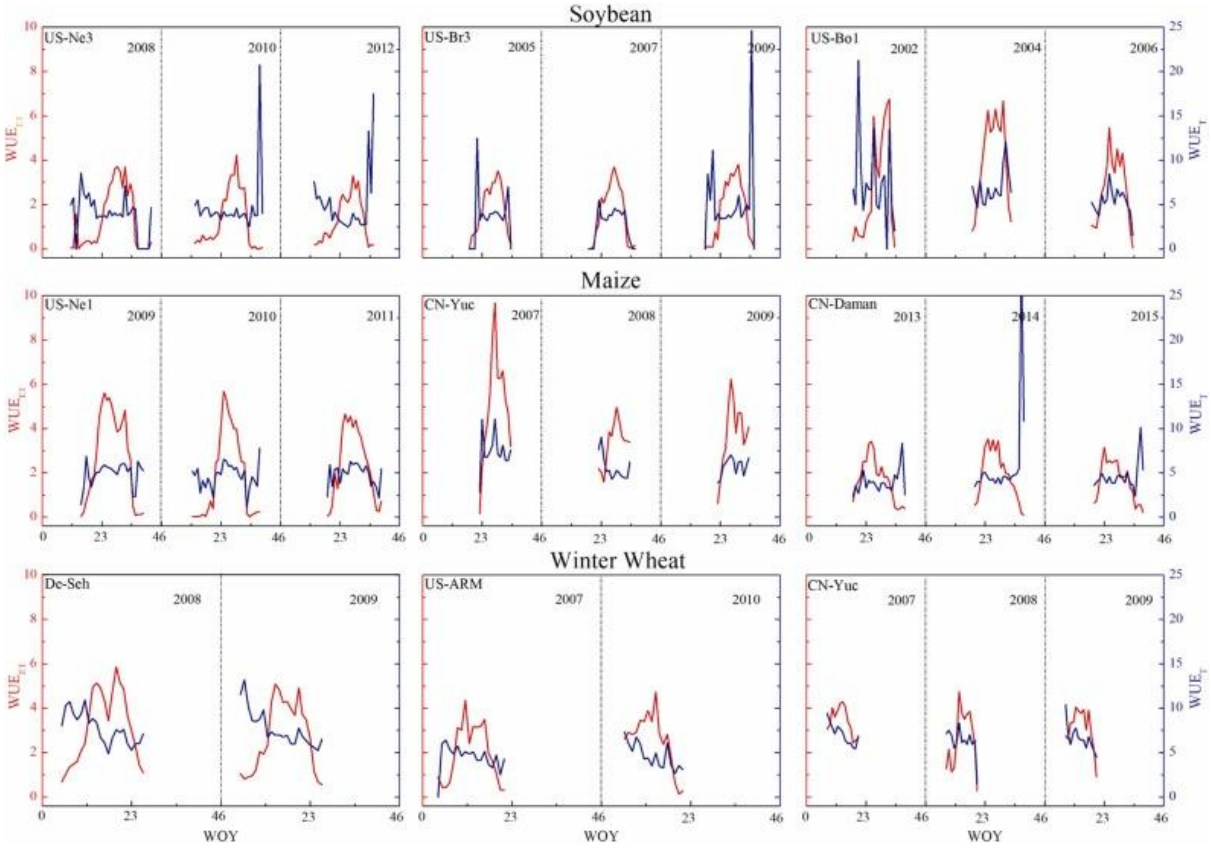

Fig. 7. The variability of ecosystem water use efficiency (WUEET), and canopy water use efficiency (WUET) at 8-day time scale for soybean, maize and winter wheat flux sites.

The study also compared the magnitudes of multi-year mean WUE_T and WUE_{ET} for three typical croplands (Fig. 8). Since WUE_{ET} represented water use efficiency of the entire ecosystem including water consumption by soil evaporation, whereas WUE_T was only contributed by vegetation transpiration component, WUE_T was apparently larger than WUE_{ET} for all crops. Overall, without distinguishing crop types, the mean WUE_{ET} was approximately half of WUE_T (2.2 g C kg^{-1} H_2O vs 5.0 g C kg^{-1} H_2O). Additionally, it seems that both WUE_T and WUE_{ET} of the C_4 cropland (maize) were slightly bigger than the C_3 croplands including soybean and winter wheat ranging from 2.8% to 22.2%.

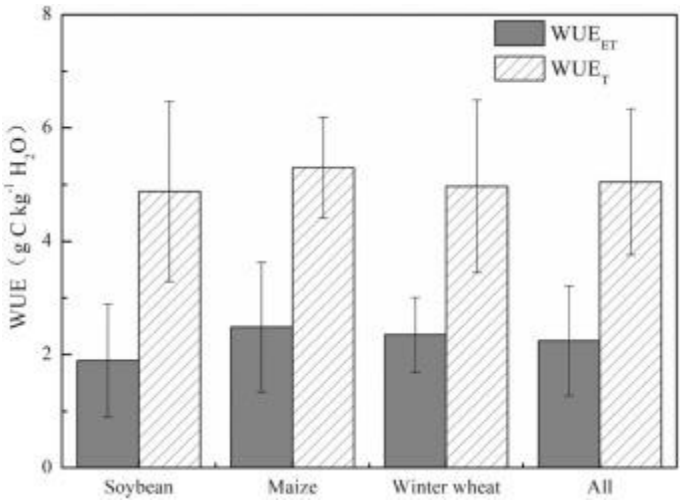

Fig. 8. Multi-year average ecosystem water use efficiency (WUEET), and canopy water use efficiency (WUET) for three typical croplands.

4. Discussion

4.1 Effect of the biotic and abiotic factors on T/ET

The ratio of transpiration to total terrestrial evapotranspiration (T/ ET) plays an important role in the hydrological cycle and in the energy budgets between the biosphere and the atmosphere (Zhou et al., 2014; Niu et al., 2019). As the primary factor controlling variations in T/ET, an increase in LAI by increasing the vegetation coverage area promotes canopy T and interception evaporation, thereby leading to the rise in ET (Piao et al., 2007; Fatichi and Pappas, 2017; Li et al., 2018). However, increasing LAI lowered the amount of energy (net radiation) reaching the soil surface, soil evaporation usually reduced, which partly offset the increase in ET associated with high LAI (Hu et al., 2009; Huang et al., 2015; Gu et al., 2018). Therefore, T and ET may have different sensitivities to the changes in LAI (Niu et al., 2019). Jiang et al. (2020) revealed the significantly positive correlations ($p < 0.01$) between daily T/ET and MODIS LAI at four representative winter wheat, paddy rice, soybean and summer maize sites, which were consistent to our results. As illustrated in Fig. 9, the highest R^2 between T/ET and LAI of maize reached up to 0.68 at 8-day time scale, followed by soybean with 0.63, and the lowest for winter wheat was 0.37. All analyses again indicated that LAI dominated the water-related ET and T cycles.

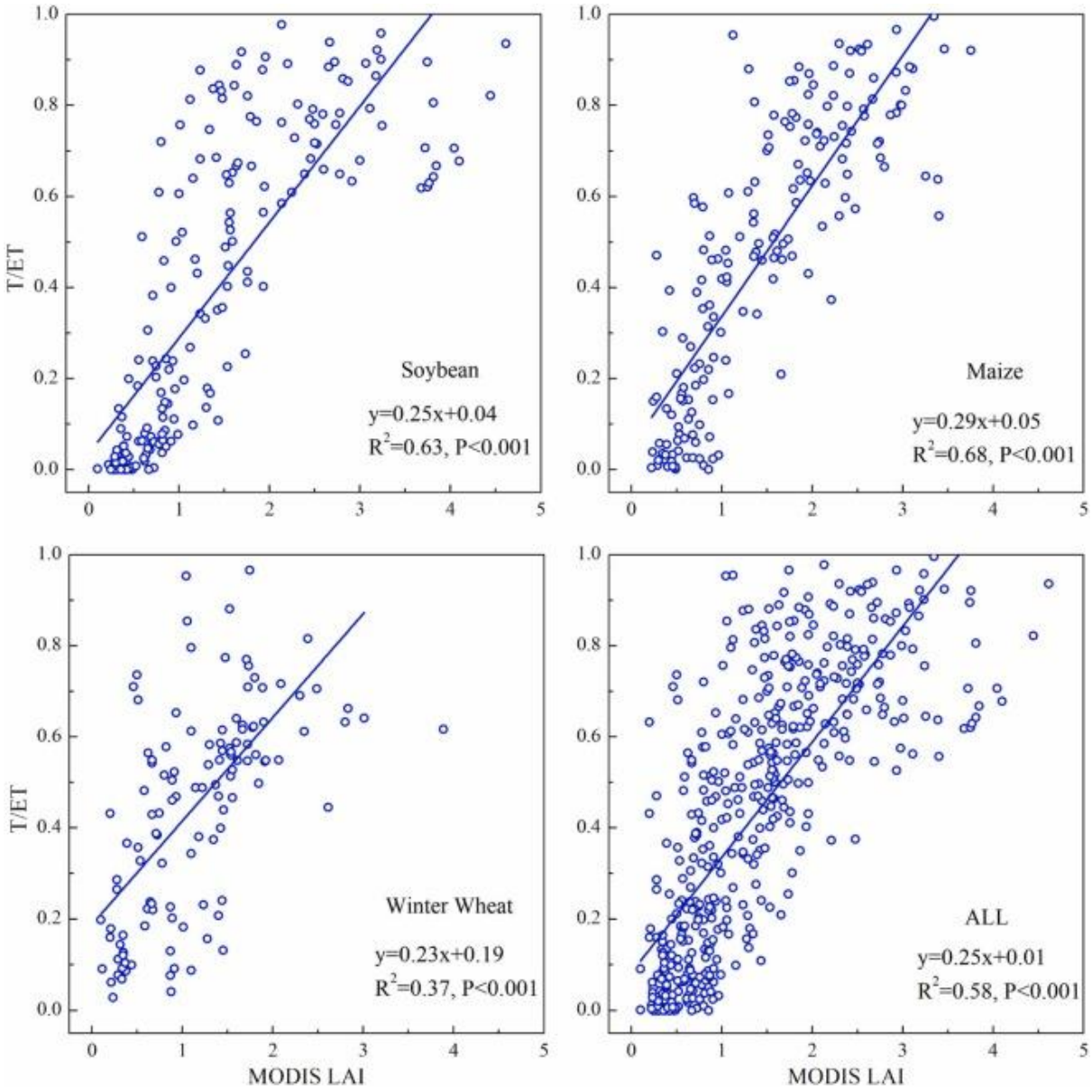

Fig. 9. The linear relationship between MODIS LAI and T/ET for each 8 day period at soybean, maize, winter wheat, and all sites.

Previous studies found that when LAI is relatively low at the early growing stage, an increase in LAI caused by crop growth will obviously enhance vegetation photosynthesis (Jiang et al., 2020), and subsequently lead to an increase in WUE; once LAI exceeds the threshold, the change in crop T/ET is limited, resulting in the insensitive response of WUE to LAI (Zhang et al., 2013a, 2013b). Thus, LAI can influence water use efficiency from canopy to ecosystem scales by adjusting the variability in T/ET (Zhang et al., 2014; Zhu et al., 2014; Hu et al., 2008; Kato et al., 2004). Besides, the abiotic factors including ambient atmospheric conditions, soil moisture, and solar radiation affected the dynamics of T/ET at daily or seasonal scales (Good et al., 2014; Scott and Biederman, 2017; Gao et al., 2021). Meanwhile, Niu et al. (2019) suggested that temperature change is the most important factor in driving interannual T/ET trend both nationally and regionally.

4.2 Contrasting controls on WUE_T and WUE_{ET}

A deep understanding of the water-carbon relationship is critical for model development, water and carbon management, and decision- making for precision agriculture. Previous studies mostly focused on ecosystem-level water consumption and the associated water use efficiency (Gao et al., 2014; Wang et al., 2018). In this study, we investigated the difference in WUE_T and WUE_{ET} from the canopy to ecosystem scales across the typical croplands (Figs. 7 and 8). Cheng et al. (2017) indicated that the increase in carbon uptake was not accompanied by a proportional increase in ET, which was largely driven by increased WUE in terrestrial ecosystem (about 90%). By comparison with ET, Wang et al. (2018) revealed that GPP determined the variability in WUE_{ET} for croplands throughout the growing season. Li et al. (2019) also indicated that seasonal dynamics in WUE was mainly controlled by the carbon flux rather than water flux in shrubland of the northeastern Qinghai-Tibetan Plateau, China. Nevertheless, other studies suggested that GPP dominated the changes in WUE_{ET} mainly during the high water-carbon coupling strength stage (Gao et al., 2021).

Our findings are consistent with previous studies at the ecosystem level. As illustrated in Fig. 10, both GPP and ET showed significant positive correlation with WUE_{ET} ($p < 0.01$) across the typical croplands. However, compared with water flux, carbon flux played a more important role in dominating the variability in WUE_{ET}. The correlations between WUE_{ET} and GPP ranged from 0.52 at the winter wheat site to 0.91 at the maize site. Contrastingly, the correlations between WUE_{ET} and ET were apparently lower. Without distinguishing crop types, the correlations between WUE_{ET} and GPP or ET were 0.85 and 0.45, respectively. During the early and late growing seasons, water and carbon fluxes were primarily determined by the biotic factor such as LAI and varied towards a concurrent trend. But the amplitude of variation of the carbon flux was slightly larger than that of the water flux, mainly due to soil evaporation (Fig. 5).

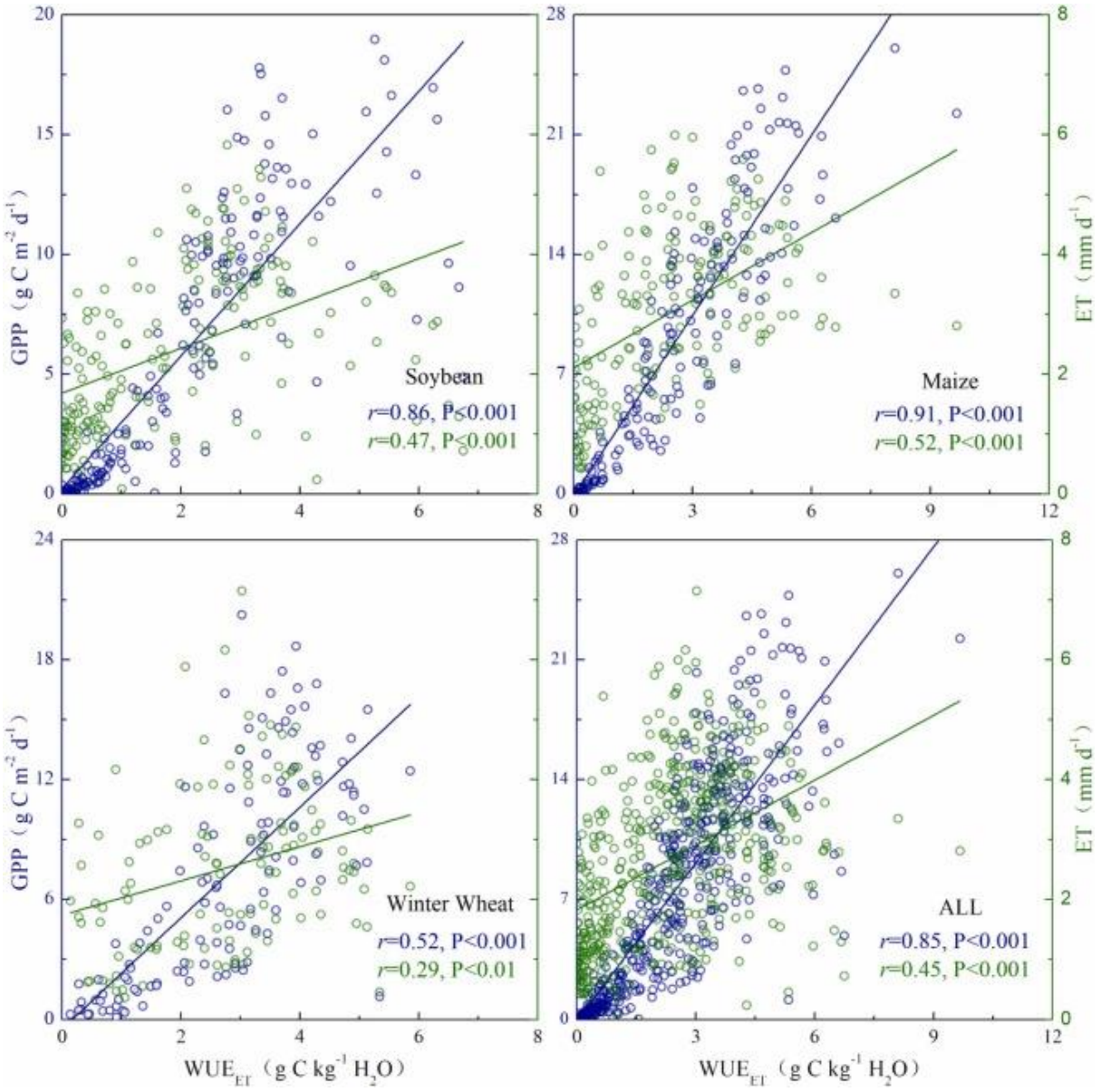

Fig. 10. The linear relationship between GPP, ET and WUEET for each 8 day period at soybean, maize, winter wheat, and all cropland sites.

In addition, our finding further evidenced that the canopy-scale WUE_T had no significant linear correlations with GPP or T in Fig. 11. As GPP and T varied, WUE_T approached a constant value, which indicated that both GPP and T changed in the same proportion. The coordinated relationship between GPP and T proved that the seasonal variation of WUE_T was not related to these two parameters, and recognized as the intrinsic characteristic of the plant functional types (Broeckx et al., 2014). As important components of water and carbon fluxes, both T and GPP are regulated and closely related through gas diffusion via plant stomata (Gao et al., 2021; Mathias and Thomas, 2021). Therefore, water and carbon fluxes are inherently coupled at the canopy scale.

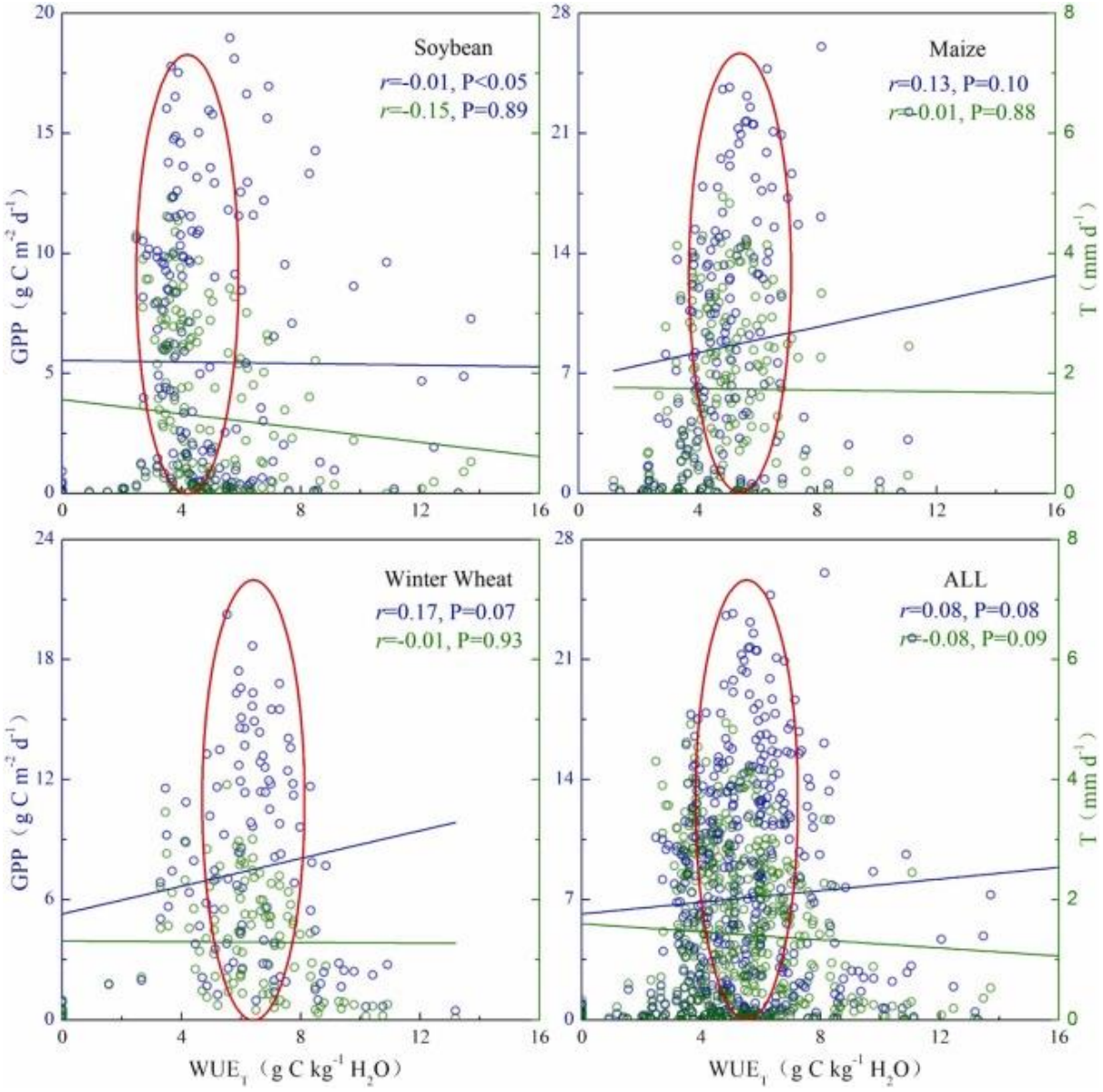

Fig. 11. The linear relationship between GPP, T and WUET for each 8 day period at soybean, maize, winter wheat, and all cropland sites.

5. Conclusions

In this study, we applied the uWUE method for ET partitioning to three typical cropland ecosystems, and quantified the variability in water fluxes from the canopy scale to ecosystem scale as well as their associated water use efficiency. As a proxy for the transpiration ratio, T/ ET exhibited a single-peak curve over all three crops. Time-series MODIS LAI data performed great potential for remotely retrieving large-scale T/ ET pattern. Meanwhile, multiple site-years of flux data inferred that maize has the largest T/ET by 0.50, followed by soybean of 0.43 and winter wheat of 0.38, respectively. The study also indicated that both ET and T covaried with the dynamics in GPP, yet large discrepancies be- tween T and ET became narrow as crops grew. Furthermore, the relationship between GPP and T showed a linear correlation at canopy scale, whereas a nonlinear relationship existed between GPP and ET at the ecosystem scale. In addition, WUE_{ET} of croplands exhibited distinct seasonal patterns during the growing

season. Contrastingly, WUE_T kept constant as a plateau nearly throughout crop growth period, which reflected the inherently coupling relations to GPP through plant stomata at the canopy scale. Despite that the uWUE method can be used as an effective tool to estimate T/ET of croplands, further study could evaluate the performance of other methods such as isotope or lysimeter techniques for ET partitioning.

As one of the largest terrestrial biomes on the planet, the role of cropland in food security is facing serious threats from global climate change, especially for water scarcity problems. A deep understanding of the processes of cropland ET, and sustainable use of water resources is significant for global food security. Essentially, the water consumed by vegetation T is directly associated to grain production. Several management practices have been implemented to reduce the useless water consumption by bare soil in recent years. For example, planting green manure crops before spring ploughing (Sorkheh et al., 2020) and returning crop stalks to the field after harvest can largely decrease soil evaporation (Li et al., 2020). Therefore, this study is helpful for a more profound recognition of the water-carbon coupling and provides a new framework for developing water-saving agriculture.

Acknowledgments

This study was supported by the National Natural Science Foundation of China (41830648, 41771361), National Major Projects on High- Resolution Earth Observation System, China (21-Y20B01–9001-19/22) and Graduate Scientific Research and Innovation Foundation of Chongqing, China (CYS21108). Many thanks to the global FLUXNET community including AmeriFlux, AsiaFlux, and the European Flux Database. We are also grateful to the developers of MODIS products provided by NASA's Earth Observation System Data.

References

Ailin, F., Honglin, H., Limin, L., Xiaoli, R., Li, Z., Rong, G., Fenghua, Z., 2016. A Comparison of Multiple Phenology Data Sources for Estimating the Main Phenological Phases of Winter Wheat in Yucheng Station. Remote Sens. Tech. Appl. 31, 958–965.

Alton, P.B., 2016. The sensitivity of models of gross primary productivity to meteorological and leaf area forcing: a comparison between a Penman–Monteith ecophysiological approach and the MODIS light-use efficiency algorithm. Agric. For. Meteorol. 218–219, 11–24.

Baldocchi, D.D., Ryu, Y., 2011. A synthesis of forest evaporation fluxes–from days to years–as measured with eddy covariance. Forest Hydrology and Biogeochemistry. Springer, pp. 101–116.

Barr, A., Richardson, A., Hollinger, D., Papale, D., Arain, M., Black, T., Bohrer, G., Dragoni, D., Fischer, M., Gu, L., 2013. Use of change-point detection for friction–velocity threshold evaluation in eddy-covariance studies. Agric. For. Meteorol. 171, 31–45.

Berry, J.A., Beerling, D.J., Franks, P.J., 2010. Stomata, key players in the earth system, past and present. Curr. Opin. Plant Biol. 13 (3), 232–239.

Blum, A., 2005. Drought resistance, water-use efficiency, and yield potential - are they compatible, dissonant, or mutually exclusive? Aust. J. Agric. Res. 56, 1159–1168.

Broeckx, L.S., Fichot, R., Verlinden, M.S., Ceulemans, R., 2014. Seasonal variations in photosynthesis, intrinsic water-use efficiency and stable isotope composition of poplar leaves in a short-rotation plantation.Tree Physiol. 34, 701–715.

Cai, Z., Jönsson, P., Jin, H., Eklundh, L., 2017. Performance of smoothing methods for reconstructing NDVI time-series and estimating vegetation phenology from MODIS data. Remote Sens. 9.

Cheng, L., Zhang, L., Wang, Y.-P., Canadell, J.G., Chiew, F.H.S., Beringer, J., Li, L., Miralles, D.G., Piao, S., Zhang, Y., 2017. Recent increases in terrestrial carbon uptake at little cost to the water cycle. Nat. Commun. 8, 110.

Chu, H., Baldocchi, D.D., Poindexter, C., Abraha, M., Desai, A.R., Bohrer, G., Arain, M.A., Griffis, T., Blanken, P.D., O'Halloran, T.L., 2018. Temporal dynamics of aerodynamic canopy height derived from eddy covariance momentum flux data across North American flux networks. Geophys. Res. Lett. 45, 9275–9287.

Dietzel, R., Liebman, M., Ewing, R., Helmers, M., Horton, R., Jarchow, M., Archontoulis, S., 2016. How efficiently do corn-and soybean-based cropping systems use water? A systems modeling analysis. Glob. Change Biol. 22 (2), 666–681.

Drake, J.E., Power, S.A., Duursma, R.A., Medlyn, B.E., Aspinwall, M.J., Choat, B., Creek, D., Eamus, D., Maier, C., Pfautsch, S., Smith, R.A., Tjoelker, M.G., Tissue, D. T., 2017. Stomatal and non-stomatal limitations of photosynthesis for four tree species under drought: A comparison of model formulations. Agric. For. Meteorol. 247, 454–466.

Fang, H., Baret, F., Plummer, S., Schaepman-Strub, G., 2019. An overview of global leaf area index (LAI): methods, products, validation, and applications. Rev. Geophys. 57, 739–799.

Fatichi, S., Pappas, C., 2017. Constrained variability of modeled T:ET ratio across biomes. Geophys. Res. Lett. 44, 6795–6803.

Fisher, J.B., Tu, K.P., Baldocchi, D.D., 2008. Global estimates of the land–atmosphere water flux based on monthly AVHRR and ISLSCP-II data, validated at 16 FLUXNET sites. Remote Sens. Environ. 112, 901–919.

Gao, L., Kang, S., Bai, X., Li, S., Niu, J., Ding, R., 2021. Water-carbon relationships and variations from the canopy to ecosystem scale in a sparse vineyard in the northwest China. J. Hydrol. 600, 126469.

Gao, Y., Zhu, X., Yu, G., He, N., Wang, Q., Tian, J., 2014. Water use efficiency threshold for terrestrial ecosystem carbon sequestration in China under afforestation. Agric. For. Meteorol. 195–196, 32–37.

Gillies, R.R., Carlson, T.N., Cui, J., Kustas, W.P., Humes, K.S., 1997. A verification of the 'triangle' method for obtaining surface soil water content and energy fluxes from remote measurements of the Normalized Difference Vegetation Index (NDVI) and surface radiant temperature. Int. J. Remote Sens. 18, 3145–3166.

Good, S.P., Soderberg, K., Guan, K., King, E.G., Scanlon, T.M., Caylor, K.K., 2014. δ2H isotopic flux partitioning of evapotranspiration over a grass field following a water pulse and subsequent dry down. Water Resour. Res. 50, 1410–1432.

Griffis, T.J., 2013. Tracing the flow of carbon dioxide and water vapor between the biosphere and atmosphere: A review of optical isotope techniques and their application. Agric. For. Meteorol. 174–175, 85–109.

Gu, C., Ma, J., Zhu, G., Yang, H., Zhang, K., Wang, Y., Gu, C., 2018. Partitioning evapotranspiration using an optimized satellite-based ET model across biomes. Agric. For. Meteorol. 259, 355–363.

Gu, J., Li, X., Huang, C., Okin, G.S., 2009. A simplified data assimilation method for reconstructing time-series MODIS NDVI data. Adv. Space Res. 44, 501–509.

Guo, L., An, N., Wang, K., 2016. Reconciling the discrepancy in ground- and satellite-observed trends in the spring phenology of winter wheat in China from 1993 to 2008. J.

Geophys. Res. Atmos. 121, 1027–1042.

Hu, Z., Yu, G., Fu, Y., Sun, X., Li, Y., Shi, P., Wang, Y., Zheng, Z., 2008. Effects of vegetation control on ecosystem water use efficiency within and among four grassland ecosystems in China. Glob. Change Biol. 14, 1609–1619.

Hu, Z., Yu, G., Zhou, Y., Sun, X., Li, Y., Shi, P., Wang, Y., Song, X., Zheng, Z., Zhang, L., 2009. Partitioning of evapotranspiration and its controls in four grassland ecosystems: Application of a two-source model. Agric. For. Meteorol. 149, 1410–1420.

Huang, M., Piao, S., Sun, Y., Ciais, P., Cheng, L., Mao, J., Poulter, B., Shi, X., Zeng, Z., Wang, Y., 2015. Change in terrestrial ecosystem water-use efficiency over the last three decades. Glob. Change Biol. 21, 2366–2378.

Ito, A., Inatomi, M., 2012. Water use efficiency of the terrestrial biosphere, a model analysis focusing on interactions between the global carbon and water cycles. J. Hydrometeorol. 13 (2), 681–694.

Jiang, S., Liang, C., Cui, N., Zhao, L., Liu, C., Feng, Y., Hu, X., Gong, D., Zou, Q., 2020. Water use efficiency and its drivers in four typical agroecosystems based on flux tower measurements. Agric. For. Meteorol. 295, 108200.

Jiang, Y., 2009. China's water scarcity. J. Environ. Manag. 90, 3185–3196. John, P., Tim, P., 2016. AmeriFlux US-Br3 Brooks Field Site 11- Ames, Ver. 1–1, AmeriFlux AMP, (Dataset).

Kato, T., Kimura, R., Kamichika, M., 2004. Estimation of evapotranspiration, transpiration ratio and water-use efficiency from a sparse canopy using a compartment model. Agric. Water Manag. 65, 173–191.

Knyazikhin, Y., Martonchik, J.V., Myneni, R.B., Diner, D.J., Running, S.W., 1998. Synergistic algorithm for estimating vegetation canopy leaf area index and fraction of absorbed photosynthetically active radiation from MODIS and MISR data. J. Geophys. Res. Atmos. 103, 32257–32275.

Lan, X., Liu, Z., Chen, X., Lin, K., Cheng, L., 2021. Trade-off between carbon sequestration and water loss for vegetation greening in China. Agric. Ecosyst. Environ. 319, 107522.

Li, X., Gentine, P., Lin, C., Zhou, S., Sun, Z., Zheng, Y., Liu, J., Zheng, C., 2019. A simple and objective method to partition evapotranspiration into transpiration and evaporation at eddy-covariance sites. Agric. For. Meteorol. 265, 171–182.

Li, X.-X., Li, Z., 2018. The impact of anxiety on the progression of mild cognitive impairment to dementia in Chinese and English data bases: a systematic review and meta-analysis. Int. J. Geriatr. Psychiatry 33, 131–140.

Li, Y., Chen, H., Feng, H., Wu, W., Zou, Y., Chau, H.W., Siddique, K.H., 2020. Influence of straw incorporation on soil water utilization and summer maize productivity: a five-year field study on the Loess Plateau of China. Agric. Water Manag. 233, 106.

Liu, C., Zhang, X., Zhang, Y., 2002. Determination of daily evaporation and evapotranspiration of winter wheat and maize by large-scale weighing lysimeter and micro-lysimeter. Agric. For. Meteorol. 111, 109–120.

Liu, S., Xu, Z., 2018. Micrometeorological methods to determine evapotranspiration. Obs. Meas. Ecohydrol. Process.

Liu, Y., Zhou, Y., Ju, W., Chen, J., Wang, S., He, H., Wang, H., Guan, D., Zhao, F., Li, Y., Hao, Y., 2013. Evapotranspiration and water yield over China's landmass from 2000 to 2010. Hydrol. Earth Syst. Sci. 17, 4957–4980.

Liu, Z.Y., Tornros, T., Menzel, L., 2016. A probabilistic prediction network for hydrological drought identification and environmental flow assessment. Water Resour. Res. 52, 6243–6262.

Lu, Y., Williams, I.N., Bagley, J.E., Torn, M.S., Kueppers, L.M., 2017. Representing winter wheat in the Community Land Model (version 4.5). Geosci. Model Dev. 10, 1873–1888.

Mathias, J.M., Thomas, R.B., 2021. Global tree intrinsic water use efficiency is enhanced by increased atmospheric CO_2 and modulated by climate and plant functional types. Proc. Natl. Acad. Sci. 118.

Maxwell, R.M., Condon, L.E., 2016. Connections between groundwater flow and transpiration partitioning. Science 353, 377.

Meyers, T.P., Hollinger, S.E., 2004. An assessment of storage terms in the surface energy balance of maize and soybean. Agric. For. 125, 105–115.

Monfreda, C., Ramankutty, N., Foley, J.A., 2008. Farming the planet: 2. Geographic distribution of crop areas, yields, physiological types, and net primary production in the year 2000. Glob. Biogeochem. Cycles 22.

Mu, Q., Zhao, M., Running, S.W., 2011. Improvements to a MODIS global terrestrial evapotranspiration algorithm. Remote Sens. Environ. 115 (8), 1781–1800.

Nelson, J.A., Ṕerez-Priego, O., Zhou, S., Poyatos, R., Zhang, Y., Blanken, P.D., Gimeno, T. E., Wohlfahrt, G., Desai, A.R., Gioli, B., 2020. Ecosystem transpiration and evaporation: insights from three water flux partitioning methods across FLUXNET sites. Glob. Change Biol. 26, 6916–6930.

Niu, S.L., Xing, X.R., Zhang, Z., Xia, J.Y., Zhou, X.H., Song, B., Li, L.H., Wan, S.Q., 2011. Water-use efficiency in response to climate change: from leaf to ecosystem in a temperate steppe. Glob. Change Biol. 17, 1073–1082.

Niu, Z., He, H., Zhu, G., Ren, X., Zhang, L., Zhang, K., Yu, G., Ge, R., Li, P., Zeng, N., Zhu, X., 2019. An increasing trend in the ratio of transpiration to total terrestrial evapotranspiration in China from 1982 to 2015 caused by greening and warming. Agric. For. Meteorol. 279, 107701.

Novick, K.A., Ficklin, D.L., Stoy, P.C., Williams, C.A., Bohrer, G., Oishi, A.C., Papuga, S. A., Blanken, P.D., Noormets, A., Sulman, B.N., 2016. The increasing importance of atmospheric demand for ecosystem water and carbon fluxes. Nat. Clim. Change 6, 1023–1027.

Paul-Limoges, E., Wolf, S., Schneider, F.D., Longo, M., Moorcroft, P., Gharun, M., Damm, A., 2020. Partitioning evapotranspiration with concurrent eddy covariance measurements in a mixed forest. Agric. For. Meteorol. 280, 107786.

Pettorelli, N., Vik, J.O., Mysterud, A., Gaillard, J.-M., Tucker, C.J., Stenseth, N.C., 2005. Using the satellite-derived NDVI to assess ecological responses to environmental change. Trends Ecol. Evol. 20, 503–510.

Piao, S., Friedlingstein, P., Ciais, P., de Noblet-Ducoudŕe, N., Labat, D., Zaehle, S., 2007. Changes in climate and land use have a larger direct impact than rising CO_2 on global river runoff trends. Proc. Natl. Acad. Sci. 104, 15242–15247.

Rafi, Z., Merlin, O., Le Dantec, V., Khabba, S., Mordelet, P., Er-Raki, S., Amazirh, A., Olivera-Guerra, L., Ait Hssaine, B., Simonneaux, V., Ezzahar, J., Ferrer, F., 2019. Partitioning evapotranspiration of a drip-irrigated wheat crop: inter-comparing eddy covariance-, sap flow-, lysimeter- and FAO-based methods. Agric. For. Meteorol. 265, 310–326.

Reichstein, M., Falge, E., Baldocchi, D., Papale, D., Aubinet, M., Berbigier, P.,

Bernhofer, C., Buchmann, N., Gilmanov, T., Granier, A., Grünwald, T., Havŕánková, K., Ilvesniemi, H., Janous, D., Knohl, A., Laurila, T., Lohila, A., Loustau, D., Matteucci, G., Meyers, T., Miglietta, F., Ourcival, J.-M., Pumpanen, J., Rambal, S., Rotenberg, E., Sanz, M., Tenhunen, J., Seufert, G., Vaccari, F., Vesala, T., Yakir, D., Valentini, R., 2005. On the separation of net ecosystem exchange into assimilation and ecosystem respiration: review and improved algorithm. Glob. Change Biol. 11, 1424–1439.

Reichstein, M., Moffat, A., Wutzler, T., Sickel, K., 2014. REddyProc: Data processing and plotting utilities of (half-) hourly eddy-covariance measurements. R package version 0.6–0/r9 755.

Ren, X.L., Lu, Q.Q., He, H.L., Zhang, L., Niu, Z.G., 2019. Spatio-temporal variations of the ratio of transpiration to evapotranspiration in forest ecosystems along the North-South Transect of Eastern China. Acta Geogr. Sin. 74, 63–75.

Romero-Aranda, M.R., Jurado, O., Cuartero, J., 2006. Silicon alleviates the deleterious salt effect on tomato plant growth by improving plant water status. J. Plant Physiol. 163, 847–855.

Scanlon, T.M., 2008. Partitioning water vapor and carbon dioxide fluxes using correlation analysis. AGU Fall Meet. Abstr.

Scanlon, T.M., Albertson, J.D., 2004. Canopy scale measurements of CO_2 and water vapor exchange along a precipitation gradient in southern Africa. Glob. Change Biol. 10 (3), 329–341.

Scanlon, T.M., Kustas, W.P., 2010. Partitioning carbon dioxide and water vapor fluxes using correlation analysis. Agric. . Meteorol. 150, 89–99.

Schlesinger, W.H., Jasechko, S., 2014. Transpiration in the global water cycle. Agric. For. Meteorol. 189–190, 115–117.

Schmidt, M., Reichenau, T.G., Fiener, P., Schneider, K., 2012. The carbon budget of a winter wheat field: An eddy covariance analysis of seasonal and inter-annual variability. Agric. For. Meteorol. 165, 114–126.

Scott, R.L., Biederman, J.A., 2017. Partitioning evapotranspiration using long-term carbon dioxide and water vapor fluxes. Geophys. Res. Lett. 44, 6833–6840.

Song, Y., Jin, L., Zhu, G.F., Ma, M.G., 2016. Parameter estimation for a simple two-source evapotranspiration model using Bayesian inference and its application to remotely sensed estimations of latent heat flux at the regional scale. Agric. For. Meteorol. 230, 20–32.

Song, Z., Yang, H., Huang, X., Yu, W., Huang, J., Ma, M., 2021. The spatiotemporal pattern and influencing factors of land surface temperature change in China from 2003 to 2019. Int. J. Appl. Earth Obs. Geoinf. 104, 102537.

Sorkheh, M., Zaefarian, F., Gharineh, M.H., 2020. Effect of green manure under different conditions of tillage on weed characteristics and corn (Zea mays L.) yield. J. Plant Prod. 43, 281–294.

Suyker, A., 2021. AmeriFlux US-Ne3 Mead-rainfed maize-soybean rotation site. Dataset. Tang, X., Li, H., Desai, A.R., Nagy, Z., Luo, J., Kolb, T.E., Olioso, A., Xu, X., Yao, L., Kutsch, W., Pilegaard, K., Köstner, B., Ammann, C., 2014. How is water-use efficiency of terrestrial ecosystems distributed and changing on Earth? Sci. Rep. 4, 7483.

Tang, X.G., Li, H.P., Griffis, T.J., Xu, X.B., Ding, Z., Liu, G.H., 2015. Tracking ecosystem water use efficiency of cropland by exclusive use of MODIS EVI data. Remote Sens. 7, 11016–11035.

Tang, X.G., Li, H.P., Ma, M.G., Yao, L., Peichl, M., Arain, A., Xu, X.B., Goulden, M., 2017. How do disturbances and climate effects on carbon and water fluxes differ between multi-aged and even-aged coniferous forests? Sci. Total Environ. 599, 1583–1597.

Tilden, M., 2016. AmeriFlux US-Bo1 Bondville, Ver. 2–1, AmeriFlux AMP, (Dataset).
Ullah, H., Santiago-Arenas, R., Ferdous, Z., Attia, A., Datta, A., 2019. Chapter two - improving water use efficiency, nitrogen use efficiency, and radiation use efficiency in field crops under drought stress: a review. Adv. Agron. 156, 109–157.

Wagle, P., Skaggs, T.H., Gowda, P.H., Northup, B.K., Neel, J.P.S., 2020. Flux variance similarity-based partitioning of evapotranspiration over a rainfed alfalfa field using high frequency eddy covariance data. Agric. For. Meteorol. 285–286, 107907.

Wallace, J.S., 2000. Increasing agricultural water use efficiency to meet future food production. Agric. Ecosyst. Environ. 82, 105–119.

Wang, L., Caylor, K.K., Villegas, J.C., Barron-Gafford, G.A., Breshears, D.D., Huxman, T. E., 2010. Partitioning evapotranspiration across gradients of woody plant cover: assessment of a stable isotope technique. Geophys. Res. Lett. 37.

Wang, T., Tang, X., Chen, Z., Gu, Q., Jin, W., Ma, M., 2018. Differences in ecosystem water-use efficiency among the typical croplands. Agric. Water Manag. 209, 142–150.

Wardlow, B.D., Egbert, S.L., 2008. Large-area crop mapping using time-series MODIS 250 m NDVI data: An assessment for the US Central Great Plains. Remote Sens. Environ. 112, 1096–1116.

Xiao, W., Wei, Z., Wen, X., 2018. Evapotranspiration partitioning at the ecosystem scale using the stable isotope method—a review. Agric. Meteorol. 263, 346–361.

Xu, T., Tao, J., Wang, C., Liu, G., Chen, A., Dong, J., Dong, S., Xu, Y., 2018. Pattern of agroecosystem water use efficiency and its formation causes in China. Chin. Agric. Sci. Bull. 34, 90–98.

Yu, S., Chen, Y., Li, Q., Zhou, X., Fang, Q., Wang, J., Liu, E., Luo, Y., 2006. Feasible study on water-saving effect of wheat-maize rotation pattern. Acta Ecology Sinica 26, 2523–2531.

Yu, G.R., Wang, Q.F., Fang, H.J., 2014. Theoretical framework and relative research methods of carbon-nitrogen-water coupling cycles in terrestrial ecosystems. Fundam. Sci. Issues 34 (4), 683–698.

Zhang, L.X., Hu, Z.M., Fan, J.W., Shao, Q.Q., Tang, F.P., 2014. Advancements of the spatiotemporal dynamics in ecosystem water use efficiency at regional scale. Adv. Earth Sci. 29, 691–699.

Zhang, X., Friedl, M.A., Schaaf, C.B., 2006. Global vegetation phenology from Moderate Resolution Imaging Spectroradiometer (MODIS): Evaluation of global patterns and comparison with in situ measurements. J. Geophys. Res. Biogeosci. 111.

Zhang, X., Wang, S., Sun, H., Chen, S., Shao, L., Liu, X., 2013a. Contribution of cultivar, fertilizer and weather to yield variation of winter wheat over three decades: a case study in the North China Plain. Eur. J. Agron. 50, 52–59.

Zhang, X., Wang, Y., Sun, H., Chen, S., Shao, L., 2013b. Optimizing the yield of winter wheat by regulating water consumption during vegetative and reproductive stages under limited water supply. Irrig. Sci. 31, 1103–1112.

Zhao, S., Cong, D., He, K., Yang, H., Qin, Z., 2017. Spatial-temporal variation of drought in China from 1982 to 2010 based on a modified temperature vegetation drought index

(mTVDI). Sci. Rep. 7, 1–12.

Zhou, L., He, H.-l, Sun, X.-m, Zhang, L., Yu, G.-r, Ren, X.-l, Wang, J.-y, Zhao, F.-h, 2013. Modeling winter wheat phenology and carbon dioxide fluxes at the ecosystem scale based on digital photography and eddy covariance data. Ecol. Inf. 18, 69–78.

Zhou, S., Yu, B., Huang, Y., Wang, G., 2014. The effect of vapor pressure deficit on water use efficiency at the subdaily time scale. Geophys. Res. Lett. 41, 5005–5013.

Zhou, S., Yu, B., Huang, Y., Wang, G., 2015. Daily underlying water use efficiency for AmeriFlux sites. J. Geophys. Res. Biogeosci. 120, 887–902.

Zhou, S., Yu, B., Zhang, Y., Huang, Y., Wang, G., 2016. Partitioning evapotranspiration based on the concept of underlying water use efficiency. Water Resour. Res. 52, 1160–1175.

Zhou, S., Yu, B., Zhang, Y., Huang, Y., Wang, G., 2018. Water use efficiency and evapotranspiration partitioning for three typical ecosystems in the Heihe River Basin, northwestern China. Agric. . Meteorol. 253–254, 261–273.

Zhu, X., Yu, G., Wang, Q., Hu, Z., Han, S., Yan, J., Wang, Y., Zhao, L., 2014. Seasonal dynamics of water use efficiency of typical forest and grassland ecosystems in China. J. For. Res. 19, 70–76.

Zhu, X.-J., Yu, G.-R., Hu, Z.-M., Wang, Q.-F., He, H.-L., Yan, J.-H., Wang, H.-M., Zhang, J.-H., 2015. Spatiotemporal variations of T/ET (the ratio of transpiration to evapotranspiration) in three forests of Eastern China. Ecol. Indic. 52, 411–421.